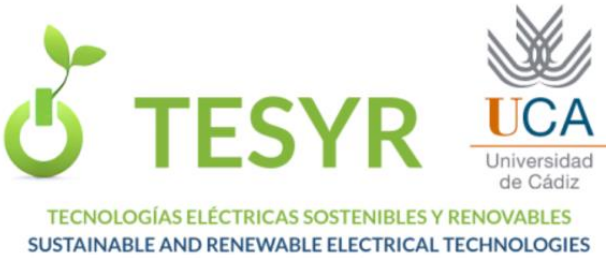

Universidad de Cádiz

Supervisory Control System for a Grid-Connected MVDC Microgrid Based on Z-Source Converters With PV, Battery Storage, Green Hydrogen System and Charging Station of Electric Vehicles

Pablo García-Triviño; Laís de Oliveira-Assís; Emanuel P.P. Soares-Ramos; Raúl Sarrias Mena; Carlos Andrés García-Vázquez; Fernández Ramírez, Luis Miguel

Published in:
IEEE Transactions on Industry Applications

DOI (link to publication from Publisher):
10.1109/TIA.2022.3233556

Publication date:
2023

Document Version:
Acceped manuscript

Citation for published version (IEEE):
P. García-Triviño, L. de Oliveira-Assís, E. P. P. Soares-Ramos, R. Sarrias-Mena, C. A. García-Vázquez and L. M. Fernández-Ramírez, "Supervisory Control System for a Grid-Connected MVDC Microgrid Based on Z-Source Converters With PV, Battery Storage, Green Hydrogen System and Charging Station of Electric Vehicles," in IEEE Transactions on Industry Applications, vol. 59, no. 2, pp. 2650-2660, March-April 2023, doi: 10.1109/TIA.2022.3233556.

IEEE TRANSACTIONS ON INDUSTRY APPLICATIONS (ID 2022-IACC-0864.R1)

Supervisory Control System for a Grid-Connected MVDC Microgrid Based on Z-Source Converters with PV, Battery Storage, Green Hydrogen System and Charging Station of Electric Vehicles

Pablo García-Triviño, Laís de Oliveira-Assís, Emanuel P. P. Soares-Ramos, Raúl Sarrias-Mena, Carlos Andrés García-Vázquez, and Luis M. Fernández-Ramírez, *Senior Member, IEEE*

***Abstract*—This paper presents a new supervisory control system (SCS) designed to maintain the power balance and obtain economic benefit by selling energy to the grid in a microgrid based on Z-source converters (ZSCs) with renewable energy, energy storage systems (ESSs), and charging station for electric vehicles (EV) connected to a medium voltage direct current (MVDC) link. The main components of the microgrid are a photovoltaic (PV) system, battery (BAT) and green hydrogen system with a fuel cell (FC), electrolyzer (LZ) and hydrogen tank as ESSs, a local grid connection and two units of fast chargers for EVs. Owing to the proposed configuration, the output voltages of the components can be adapted to the MVDC to control their output power and reduce the number of power converters compared to the common configuration without ZSCs. Thus, the configuration by itself and the SCS can be considered the main novelties of this paper. The simulation results and the hardware-in-the-loop tests show that the proposed system (ZSC-based configuration and SCS) is perfectly valid for the microgrid, and confirm the proper operation of the SCS to achieve an economic benefit from the use of the grid.**

***Index Terms*—Charging station, electric vehicles, green hydrogen system, microgrid, photovoltaics, supervisory control system, Z-source converters.**

I. Introduction

Light commercial vehicles (passenger cars and vans) account for approximately 14.5% of the total EU carbon dioxide (CO_2) emissions [1]. The use of electric vehicles (EVs) and charging stations powered by photovoltaic (PV) energy is an interesting way to reduce these emissions [2].

Hybrid charging stations can be built by combining PV systems with energy storage systems (ESSs), such as batteries (BATs) [3],[4],[5] and hydrogen systems [6][7], to satisfy the energy demanded by the charging prolife of the EVs and the energy generated by PV systems and ESSs (BAT and/or hydrogen system). In these hybrid charging stations, excess PV energy can be stored in the BAT and/or in the form of hydrogen by the electrolyzer (LZ). The PV energy deficit can be supported by the energy stored in the BAT and/or in the form of hydrogen by a fuel-cell (FC). Most charging stations use a common low-voltage DC (LVDC) bus where the energy sources are connected [8], [9]. Power converters play a key role in controlling these energy sources. Traditional two-stage conversion systems based on a DC/DC boost converter and a DC/AC voltage source inverter (VSI) are used in [10]. A DC/DC boost converter connects the PV system, ESS, and EV to a common DC bus, whereas a VSI connects the DC bus to the grid [11], [12].

Impedance source converters (ZSCs) present a configuration based on an impedance network, which allows a large voltage buck-boost feature in a single-stage conversion, integrating the stages of DC/DC boost and inverter into the same converter [13]. In traditional converters, the upper and lower devices of each phase cannot be triggered simultaneously, whereas the ZSC can handle it because of its shoot-through states. Furthermore, the ZSC does not require dead time in the gate signals, which reduces the output distortion [13]. On the other hand, the DC/DC ZSC can produce a desired output voltage irrespective of the input voltage [14] [15], which can be the variable voltage obtained from the PV system, EV, BAT, or the hydrogen system (FC and LZ).

Manuscript received July 20, 2022; revised 3 December 2022; accepted 28 December 2022. This work was partially supported by the Spain's Ministerio de Ciencia, Innovacion y Universidades (MCIU), Agencia Estatal de Investigacion (AEI), and Fondo Europeo de Desarrollo Regional (FEDER) Union Europea (UE) (grant number RTI2018-095720-B-C32) by the National Council of Technological and Scientific Development (CNPq-Brazil) and by the Federal Center for Technological Education of Minas Gerais, Brazil (process number 23062-010087/2017-51). (*Corresponding author: Luis M. Fernández-Ramírez.*)

P. García-Triviño, L. de Oliveira-Assís, C. A. García-Vázquez and L. M. Fernández-Ramírez are with the Research Group in Sustainable and Renewable Electrical Technologies (PAIDI-TEP023), Department of Electrical Engineering, Higher Technical School of Engineering of Algeciras, University of Cadiz, 11202 Algeciras, Spain (e-mail: pablo.garcia@uca.es, lais.oassis@gmail.com, carlosandres.garcia@uca.es, luis.fernandez@uca.es).

E. P. P. Soares-Ramos is with the Federal Center for Technological Education of Minas Gerais, Department of Electro-electronics, Curvelo, MG, 35790-000, Brazil (e-mail: emanuel@cefetmg.br).

R. Sarrias-Mena is with the Research Group in Sustainable and Renewable Electrical Technologies (PAIDI-TEP-023), Department of Engineering in Automation, Electronics and Computer Architecture & Networks, University of Cadiz, Higher Technical School of Engineering of Algeciras, University of Cadiz, 11202 Algeciras, Spain (e-mail: raul.sarrias@uca.es).

Color versions of one or more of the figures in this article are available online at http://ieeexplore.ieee.org

Furthermore, two different energy sources can be connected to the same ZSC without an additional DC/DC converter, and their energy flow can be controlled effectively, which is interesting for reducing the number of power converters used in hybrid charging stations [16].

In the literature, different kinds of works related to hybrid charging stations can be found. Studies that focus on optimal load scheduling cover most of the topic [17], [18]. Contrarily, the energy management within the charging station still has to be studied in depth. Improving adaptability and reliability while maximizing self-consumption and economic profitability of hybrid charging stations is a challenge that can be solved through the energy management performed by an adequate supervisory control system (SCS) [19]. Decentralized SCS applied to hybrid charging stations were presented in [3][4] and [20] in order to reduce the peak power generated by the grid. In [3], the authors developed a SCS based on model predictive control. A similar approach was carried out in [4], where the decentralized SCS was also presented, but using classical proportional-integral (PI) controllers to control the key parameter of the system, that is, the medium-voltage DC (MVDC) bus voltage. Reference [20] proposed a SCS (control-algorithm based) to evaluate a hybrid fast charging station with the aim of reducing peak demand during charging periods. In general, the three previous SCS provided reliable results minimizing the number of operations and the demand from the grid. However, the cost of the energy consumed from the grid was not taken into account. In [6], the SCS was designed from a long-term perspective with the aim of optimizing the utilization cost of the charging station for a 25 years simulation. The results presented were satisfactory. Nevertheless, neither the dynamic behaviour of the system nor the cost of the energy obtained from the grid were considered. A rule-based SCS was proposed in [21] to minimize the use of utility grid power and store PV power when the EVs are not connected for charge. The proposed SCS was validated by simulations using MATLAB-Simulink models and by experimental tests in the laboratory. The SCS maintained a constant DC bus voltage under all the modes of operation, including cases of utility grid overloading, low irradiation of PV systems, or temporary interruption of ESS. Again, the cost of the grid energy was not considered, and the results shown only covered two-seconds long simulations. A SCS for an EV charging station with a hybrid ESS comprising a flywheel and BAT was presented in [22]. The SCS was based on the voltage droop control, including hysteresis controllers, to avoid frequent switching among the control modes. The simulation results (maximum duration of 14 s) showed that the hybrid ESS had an obvious effect on the smooth transition among the modes of operation, and the SCS worked satisfactorily under different operating conditions.

The SCS in [23]–[27] considered the cost of the grid energy consumption in the decision-making process. In [23], the authors presented a SCS based on a leader-followers game to provide regulation reserves for power systems. Although the authors did not develop the SCS for charging station with a specific configuration, the results (several hours of simulation were studied) showed that the SCS was able to avoid heavy load of the system. A hierarchical predictive control algorithm for multi-port high-scale charging stations was developed in [24]. This algorithm can provide real-time energy management for charging stations, decide charging rates for the ESS and support the grid voltage. Up to 60 min of simulation were studied. The results showed that the proposed SCS was able to meet the grid constraints in terms of ramp-rate limit. On the other hand, due to the sample time of the SCS, the peak powers of the components and their dynamics could not be seen clearly. Reference [25] introduced a new type of charging station with solid-state transformer, and developed a rule-based SCS. Despite the fact that an ESS was not included in the charging station, it was shown that the SCS could provide bidirectional frequency regulation throughout several minutes of simulation. However, the lack of an ESS implies a higher dependency on the grid to provide or absorb power imbalances between generation and demand, which may harm the economically optimal operation of the charging station. Two similar configurations of the hybrid charging stations with an ESS and PV system were shown in [26] and [27]. Reference [26] presented a consecutive horizon-based energy management strategy, and [27] described a SCS based on a virtual energy hub. In both works, the long-term simulations showed the suitability of the SCSs for the proposed configurations. As in other references, and due to the sample time used, the power peaks in system were not represented in the results.

All the references above have in common the overall configuration of the hybrid charging station. In general, all configurations include a DC bus, and the components are connected to it through conventional power converters: buck or boost DC/DC converters in the case of the renewable energy generators or the ESS, and a voltage source inverter in the case of the grid. Besides, except for [6] and [22], a single ESS was considered. In hybrid systems, integrating two ESS means extra complexity regarding their energy management and control, which must be addressed by the SCS.

This paper presents a new configuration for a hybrid charging station for EVs, where all the energy sources are connected to a common MVDC bus through ZSCs. The PV system, hydrogen system, and EVs use a DC/DC ZSC for their connection to the MVDC bus. The grid connection of the MVDC bus is achieved through a DC/AC quasi-Z-source inverter (qZSI), which integrates a BAT without an additional DC/DC converter. In comparison to the typical configuration without ZSCs, the proposed configuration allows adapting the output voltage of each component and controlling their power while reducing the number of power converters.

Therefore, several scientific contributions and novelties can be considered in the present work. The main novelties deal with the configuration of the hybrid charging station: 1) The number of power converters needed is reduced with the use of ZSCs, and the impedance network of the converter creates a common DC bus and a DC connection point for the BAT, and 2) two different ESS technologies are integrated, i.e. a battery and a hydrogen system. An additional novelty of this study is the SCS. A new SCS based on the levels of energy in the BAT and the hydrogen tank is designed to maintain the power balance in the hybrid charging station, control the levels of energy in the ESS, and make an economic benefit by selling energy to the local grid.

The remainder of this paper is organized as follows. The PV/BAT/Hydrogen-powered hybrid charging station for EVs under study is detailed in Section II. The SCS proposed for the energy management of the hybrid charging station is described in Section III. A fuzzy-logic-based system and an energy dispatch system comprise the SCS. Section IV shows and discusses the simulation and experimental results. Finally, the main findings are summarized in Section V.

II. Grid- connected MVDC Microgrid with PV, BAT, Hydrogen System and Charging Station of EVs

The aim of the MVDC microgrid is to supply the energy required by the EVs connected to it. Although there is a connection with the local grid, under normal conditions, the microgrid works as a stand-alone system. Only in the case where the power balance in the charging station cannot be kept by the PV panels or the ESS, the grid participates to guarantee this balance, avoiding any functional problem.

Fig. 1 shows the entire configuration of the proposed MVDC microgrid for the EV charging station. The system integrates two fast-charging units that incorporate an off-board charger unit with a DC/DC ZSC to control the charging of each EV (EV charging mode 4, IEC61851-1 [28]). The main source of the system, the PV system, must have a peak power above the rated power of the charging station (two fast-charging units of 50 kW each). Thus, the peak PV power is 186 kW (composed of the panels from [29]). In addition, there are two ESSs. The first is a lead-acid BAT, which helps the PV system supply the energy required by the charging station [30]. The second ESS, the hydrogen system, helps the system when working in the isolated mode (normal condition). It provides the necessary energy to the system when the energy generated by the PV system and the BAT is insufficient. Thus, the hydrogen system uses unidirectional energy systems (FC and LZ) as a bidirectional ESS with the help of a hydrogen tank. Therefore, six modules of the FC from [31] with a peak power of 66 kW, a hydrogen generation system (LZ from [32]) with a rated power of 176 kVA, and a metal hydrogen tank of 450 kg are used in this work.

The PV system, BAT, and grid are connected through a qZSI, which includes an impedance network and an inverter [33]. The PV system is connected to the DC side, the grid to the AC side, and the BAT is connected in parallel with the impedance network. On the other hand, the impedance network is used as the common connection point in MVDC (around 1800 V) for the other ZSCs. These converters are used because of their advantages in adapting the voltage levels and reducing the number of power converters [13]. Thus, three ZSC developed in [15] have been considered in this work: one ZSC for the hydrogen system and two ZSC for the fast charging units.

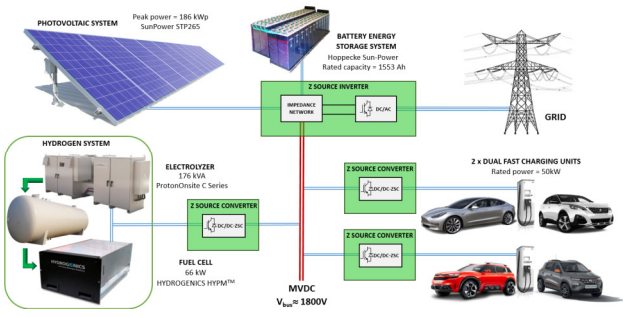

Fig. 1. Proposed configuration for the grid-connected MVDC microgrid based on ZSCs with PV, BAT, hydrogen system and EV charging station

The components of the grid-connected MVDC microgrid under study have been modelled using trusted models widely adopted in the literature. The PV system is modelled by a single-diode model, which uses a current source with a diode in parallel to model an ideal PV cell, with a series and a parallel resistance. This model is extensively employed because it is easy to implement, the parameters can be easily derived from the commercial datasheet, and it achieves suitable results to represent the real behaviour of PV cells [3]. The BAT behaviour is modelled with the model included in the Simscape Electrical toolbox of Simulink, which is composed of a variable voltage source with a resistance in series [3]. The FC is represented by an equivalent circuit, in which the output voltage is calculated from the voltage generated inside the FC and the activation, concentration, and ohmic voltage drops. This model was validated in [34]. The electrolyzer is modelled by a DC voltage source with a series resistance to reproduce the electrical performance of the device. Additionally, the hydrogen production is derived from the Faraday's law [35]. Finally, a hydrogen tank model based on the ideal gas equation is used in this work. The amount of hydrogen inside the tank is calculated from the hydrogen flow rate [36].

The main equations of the SCS are as follows. The maximum energy available in the BAT and the hydrogen tank during discharging are calculated using Eqs. (1) and (3), respectively. On the other hand, Eqs. (2) and (4) show the maximum energy that can be stored in the BAT and the hydrogen tank during the charging process, respectively.

$$E_{BAT}^{dis} = E_{BAT}^{nom} \cdot (SOC - SOC_{min}) \tag{1}$$

$$E_{BAT}^{char} = E_{BAT}^{nom} \cdot (SOC_{max} - SOC) \tag{2}$$

$$E_{H2}^{dis} = L_{H2} \cdot Q_{tank} \cdot LCV_{H2} \cdot \eta_{FC} \tag{3}$$

$$E_{H2}^{char} = (100 - L_{H2}) \cdot Q_{tank} \cdot LCV_{H2}/\eta_{LZ} \tag{4}$$

where $E_{BAT}{}^{nom}$ is the capacity of the BAT in energy terms, SOC is the state-of-charge of the BAT, L_{H2} and Q_{tank} are the current level and the capacity of the hydrogen tank, respectively; and LCV_{H2} is the low calorific value of hydrogen. In the BAT, SOC_{max} and SOC_{min} have been set to 95% and 30%, respectively. The rated power considered for the BAT in the SCS is 36.9 kW. In the hydrogen system, the maximum and minimum levels are 100% and 0%, respectively. The nominal powers of the FC and the LZ are 77 kW and 144 kW, respectively.

A new term is defined, the State of Energy (SOE). It is calculated as the ratio of the current electric energy available in the ESS to the maximum electric energy that the ESS can store.

For the proposed SCS (explained in the following section), the *SOE* provides, with a single term, real information about the current level of BAT *SOC* and L_{H2}.

$$SOE = \left(E_{H2}^{dis} + E_{BAT}^{dis}\right)/(Q_{tank} \cdot LCV_{H2} \cdot \eta_{FC} + E_{BAT}^{nom}) \quad (5)$$

III. Supervisory Control System

In the MVDC microgrid, the PV system operates at the maximum power point regardless of the SCS. Because of this, the power generated by the PV system rarely matches the load demanded by the EV. Subsequently, the ESS (BAT or hydrogen system) must work to reach the power balance. In this context, the net power (P_{net}) can be defined as the difference between the demanded load and the power generated by the PV system. The net power can have both positive and negative values. Positive values mean that the ESS (or the grid) have to inject extra power into the EV, whereas negative values mean that there is excess power from the PV system that must be absorbed by the ESS (or the grid).

The SCS developed in this work corresponds to an improved version of the simpler SCS presented in [37]. In this case, unlike the previous version, the SCS incorporates the cost of the energy exchanged with the grid (C_{grid}) to determine the operation mode of the MVDC microgrid and, therefore, the final power to be absorbed or generated by the hydrogen system and the BAT. By means of the fuzzy logic system described in

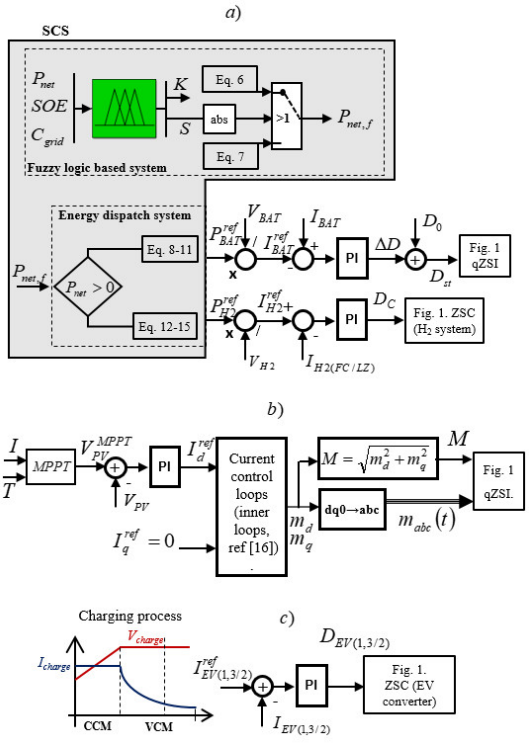

Fig. 2. Implemented control scheme: (a) SCS, battery control (from the D control of the qZSI) and hydrogen system control (from the D control of the hydrogen DC/DC ZSC), (b) MPPT of the PV panels and reactive control (from the M control of the qZSI), and (c) control of EVs (from the D control of fast charging station DC/DC ZSC)

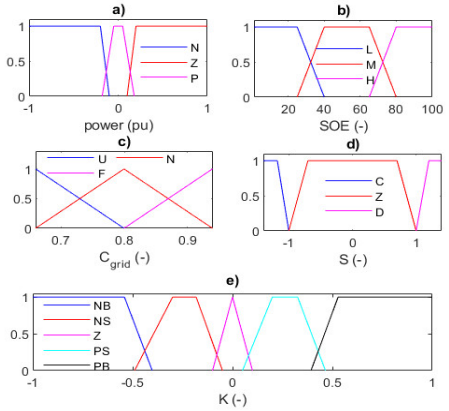

Fig. 3. Membership functions. a) P_{net}, b) *SOE*, c) C_{grid}, d) *S*, and e) *K*.

Section III.A, $P_{net,f}$ is generated from C_{grid}, P_{net} and *SOE* to make an economic profit from the use of the grid. Besides, the SCS presented herein identifies two extreme cases in the system operation which were not addressed in the previous version, i.e. low *SOE* with power demand and high *SOE* with power surplus. In [37], the SCS generated the power reference of the ESS regardless of the energy cost, and the extreme cases of *SOE* were part of the general system operation.

The main objectives of the SCS proposed in this work are to ensure the power balance within the system and to make an economic benefit from the use of the grid. To achieve these goals, the proposed SCS comprises two subsystems. The first subsystem is a fuzzy-logic-based system that modifies the value of P_{net} depending on the price of energy when using the grid. The second subsystem carries out the energy dispatch among the components of the system (BAT, hydrogen system, and grid).

This section also presents the control loops developed to control the powers generated by the SCS (Fig. 2).

A. Fuzzy-Logic-Based System

This system modifies the value of P_{net} used in the energy dispatch system to make an economic benefit from the use of the grid. As shown in Fig. 2a, the output of this system is $P_{net,f}$, which is also the input of the energy dispatch system. Thus, $P_{net,f}$ can be defined as P_{net} once modified by the fuzzy-logic-based system.

The fuzzy-logic block has three inputs and two outputs. The inputs are P_{net}, the *SOE* and the price of the energy when it is injected (sold) or absorbed (bought) by the grid, C_{grid} (Fig. 3). The outputs are two constants, *K* and *S*. *K* considers C_{grid} and allows calculating $P_{net,f}$ from P_{net} whenever the *SOE* is not excessively high or low with the goal of obtaining economic benefit by selling energy to the grid. *S* is used in extreme cases of the system (with low *SOE* and $P_{net}>0$ or high *SOE* and $P_{net}<0$). Fig. 3 shows the membership functions of the fuzzy logic system. A Mamdani-type inference is used, and 27 rules define the behaviour of the system (Table I). Finally, Fig. 2a illustrates how $P_{net,f}$ is calculated from P_{net}, *S* and *K*. According to this figure and the rules implemented, it can be observed that if $P_{net}>0$ (power must be generated by the BAT or the hydrogen system) and C_{grid} is favourable, the fuzzy-logic-based system

TABLE I. RULE BASE FOR THE FUZZY LOGIC SYSTEM.

Inputs			Outputs	
C_{grid}	SOE	P_{net}	K	S
U	L	P	NB	z
U	L	N	PB	z
U	L	Z	Z	C
U	M	P	NS	z
U	M	N	Z	z
U	M	Z	Z	z
U	H	P	PS	z
U	H	N	NS	z
U	H	Z	Z	D
N	L	P	NB	z
N	L	N	PB	z
N	L	Z	Z	**C**
N	M	P	Z	z
N	M	N	Z	z
N	M	Z	Z	z
N	H	P	PS	z
N	H	N	NB	z
N	H	Z	Z	D
F	L	P	Z	z
F	L	N	Z	z
F	L	Z	Z	C
F	M	P	PS	z
F	M	N	NB	z
F	M	Z	Z	z
F	H	P	PB	z
F	H	N	NB	z
F	H	Z	Z	D

increases P_{net} to inject power into the grid and obtain economic benefit. Similarly, if P_{net}<0 (there is an excess of power to be absorbed by the BAT or the hydrogen system) and C_{grid} is favourable, the fuzzy-logic-based system decreases P_{net} in order to absorb power from the grid and facilitate a higher charge of the ESS. Eq. (6) shows the calculation of $P_{net,f}$ when S is activated (positive or negative values), and Eq. (7) if it is not.

$$P_{net,f} = S \cdot |P_{net}| \tag{6}$$

$$P_{net,f} = P_{net}(1 + K) \tag{7}$$

Finally, with the aim of avoiding the continuous operation of this system, and therefore an unnecessary computational load for the SCS, it has been considered that the fuzzy-logic-based system modifies the value of P_{net} to $P_{net,f}$ every 10 s. This means that, every 10 s, the system reads the values of P_{net}, *SOE* and C_{grid}, generates $P_{net,f}$ and maintains the value during that period.

B. Energy Dispatch System

The input parameter of the energy dispatch system is $P_{net,f}$. This system has two main tasks. It has to decide whether the hydrogen system or the BAT (or both) generates or absorbs the net power; and it has to control the hydrogen tank level and the BAT SOC. The SCS applies a proportional distribution of the net power between the ESSs by considering the maximum available energy and the maximum energy to be stored in the BAT and the hydrogen tank (E_{BAT}^{dis}, E_{BAT}^{char}, E_{H2}^{dis}, E_{H2}^{char}). In other words, the difference between the current value of the SOC and the hydrogen tank and their minimum and maximum values (previously defined) are transformed into energy terms (Eqs. (8)-(11)).

If $P_{net,f} \geq 0$, the expressions implemented by the SCS are as follows:

$$K_{BAT}^{dis} = \frac{E_{BAT}^{dis}}{E_{BAT}^{dis} + E_{H2}^{dis}} \tag{8}$$

$$K_{H2}^{dis} = 1 - K_{BAT}^{dis} \tag{9}$$

$$P_{BAT} = min\left(P_{BAT}^{max}, K_{BAT}^{dis} \cdot P_{net,f}\right) \tag{10}$$

$$P_{H2} = min\left(P_{H2}^{max}, K_{H2}^{dis} \cdot P_{net,f}, P_{net,f} - P_{BAT}\right) \tag{11}$$

where K_{BAT}^{dis} and K_{H2}^{dis} are the proportional constants for the BAT and the hydrogen system (if $P_{net,f} \geq 0$), while P_{BAT}^{max} and P_{H2}^{max} are the maximum power that the BAT and hydrogen system can generate.

Eqs. (8) and (9) calculate the proportional constants of the BAT and the hydrogen system, respectively. Eqs. (10) and (11) determine the BAT and hydrogen system power, respectively. It is important that these expressions are implemented exactly in this sequence.

Similarly, if $P_{net,f} < 0$, the expressions are as follows:

$$K_{BAT}^{char} = \frac{E_{BAT}^{char}}{E_{BAT}^{dis} + E_{H2}^{dis}} \tag{12}$$

$$K_{H2}^{char} = 1 - K_{BAT}^{char} \tag{13}$$

$$P_{BAT} = max\left(P_{BAT}^{min}, K_{BAT}^{char} \cdot P_{net}\right) \tag{14}$$

$$P_{H2} = min\left(P_{H2}^{min}, K_{H2}^{char} \cdot P_{net}, P_{net} - P_{BAT}\right) \tag{15}$$

where K_{BAT}^{char} and K_{H2}^{char} are the proportional constants for the BAT and the hydrogen system (if $P_{net,f} < 0$), while P_{BAT}^{min} and P_{H2}^{min} are the maximum powers absorbed by the BAT and the hydrogen system. Again, as in the previous case ($P_{net,f}>0$) and for a proper operation of the SCS, these expressions must be used in this order.

Finally, in any previous case, the grid power (power to be injected into the charging station or absorbed by the grid) is the difference between the net power and the ESS power.

$$P_{grid} = P_{net} - P_{H2} - P_{BAT} \tag{16}$$

C. Control Loops

The control loops used to control the power generated by the SCS, output power of the PV system (maximum power point tracking, namely MPPT), and power demanded by the EV are shown in Fig. 2.

Fig. 2a shows that the power to be generated (absorbed) by the BAT is controlled by the shoot-through cycle (D_{st}), which is applied to the qZSI by the Z-Space Vector Modulation

(ZSVM) technique. This parameter is obtained from the sum of two terms ($\Delta D + D_0$) to achieve a fast response of the system:

$$D_{st} = \Delta D + D_o \tag{17}$$

where ΔD is the output of the BAT control loop and D_o is defined by Eq. (18).

Thus, for a certain irradiance, D_o remains constant, and ΔD moves around this term to generate D_{st} and control the BAT.

On the other hand, the output power of the hydrogen system is controlled through the duty cycle of the ZSC (Fig. 2b).

$$D_0 = V_{BAT}^{nom}/(2V_{BAT}^{nom} + V_{PV}^{MPPT}) \tag{18}$$

The active power generated by the PV system injected into the grid and the reactive power are controlled by modifying the modulation index of the qZSI (M).

The direct current reference ($i_{d,ref}$) is provided by a PI controller in the outer control loop, which controls the PV active power generation. The reactive power reference is set to zero (unity power factor), so that the quadrature current reference is set to zero ($i_{q,ref}$=0). The inner loops are the current control loops, where two PI controllers regulate i_d and i_q. A detailed description of these loops can be found in [38].

Finally, Fig. 2c illustrates that the current needed to charge the EVs is controlled by the duty cycle of the ZSC (control similar to that used in the hydrogen system). The EV charging process is based on two modes or stages. The charging modes are called the constant-current mode (CCM) and constant-voltage mode (CVM). Once the EV is connected to the fast-charging unit, the charging process starts in the CCM, in which the EV is charged with a constant current (previously imposed). In this mode, the BAT voltage increases gradually. When it reaches its nominal charge voltage, the process switches to the CVM. The charging process is completed if the current is lower than 5% of the charging current for a preset time (5 min).

IV. Results and Discussion

The aim of this section is to illustrate the suitability of the SCS applied to the MVDC microgrid for the charging station under study with the configuration based on ZSCs. In this sense, several case studies were considered: 1) General system operation in Section IV.A; 2) extreme cases in Sections IV.B (low SOE with power demand), and IV.C (high SOE with power surplus); 3) comparison with the simpler SCS presented in [37] in Section IV.D; and 4) verification with experimental validation through a Hardware-in-the-loop (HIL) test in Section IV.E.

A. General System Operation

The general operation of the SCS and its viability for the hybrid charging station is evaluated through a 1200 s simulation under variable sun irradiance, with the connection of several EVs to the charging station and considering the energy cost when using the grid C_{grid} shown in Fig. 4d. With the aim of testing the SCS, C_{grid} is considered to change every 10 s. Moreover, the SCS developed in this work (denoted as F-SCS) is compared with a simpler SCS already presented in [37], in which C_{grid} is not considered (denoted as Ref-SCS).

Figs. 4a and 4b depicts, in pu (power base, 180 kW), the total power required by the charging station (sum of the EVs) and the power demanded by each EV. These powers correspond to a fast charge of the EVs, which implies a nominal power of 50 kW. The first EV is charged from 2 s to 570 s, the second EV is connected at 580 s, and the third EV is connected at 580 s. The BAT SOC of the EVs is shown in Fig. 5b. On the other hand, Fig. 4a shows the power generated by the PV system, while Fig. 4c shows P_{net} and $P_{net,f}$. The differences between both terms are due to the operation of the fuzzy-logic-based system.

Fig. 5a shows the hydrogen system (denoted as H2), BAT, and grid powers. Negative values indicate absorbed power (LZ in the case of the hydrogen system), and positive values correspond to generated power (FC). The main purpose of the

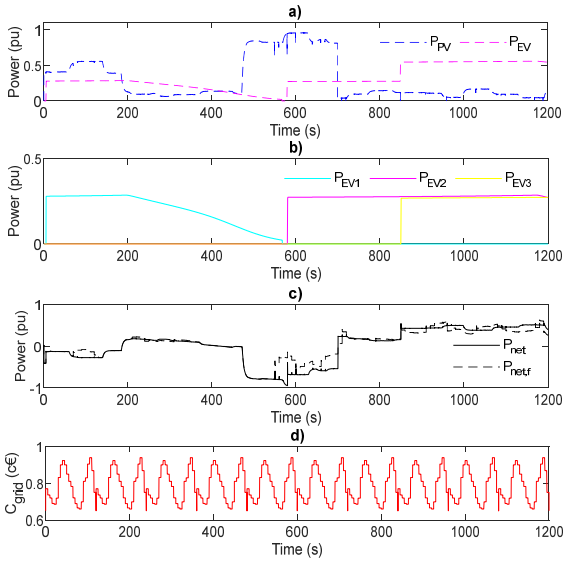

Fig. 4. a) PV system power and power demanded by the EVs, b) power demand by each EV, c) net power and $P_{net,f}$, and d) energy cost when using the grid.

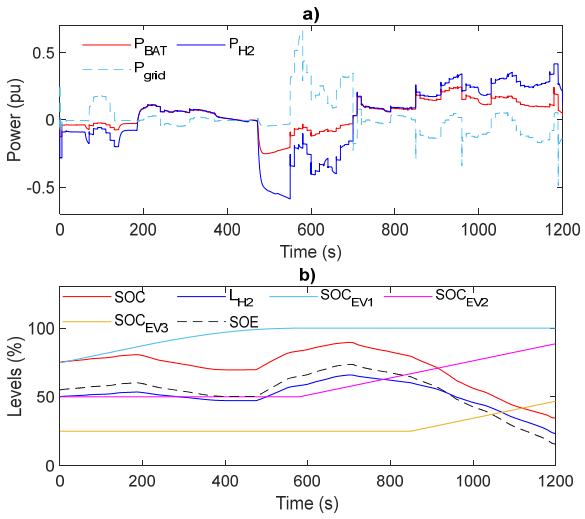

Fig. 5. Results with the proposed SCS: a) Hydrogen system, BAT and grid power, and b) BAT SOC, hydrogen tank level, state of energy, and BAT SOC of the EVs

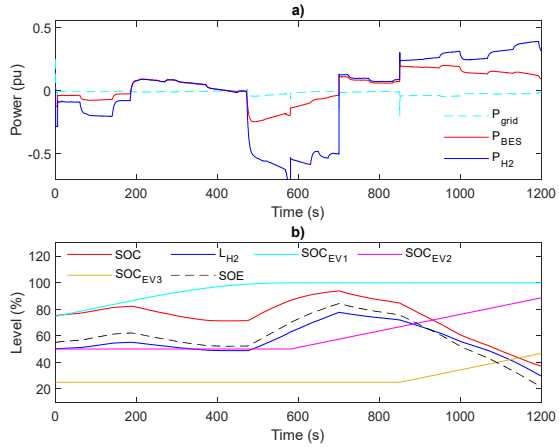

Fig. 6. Results with the Ref-SCS: a) Hydrogen system, BAT and grid power, and b) BAT SOC, hydrogen tank level, state of energy, and BAT SOC of the EVs

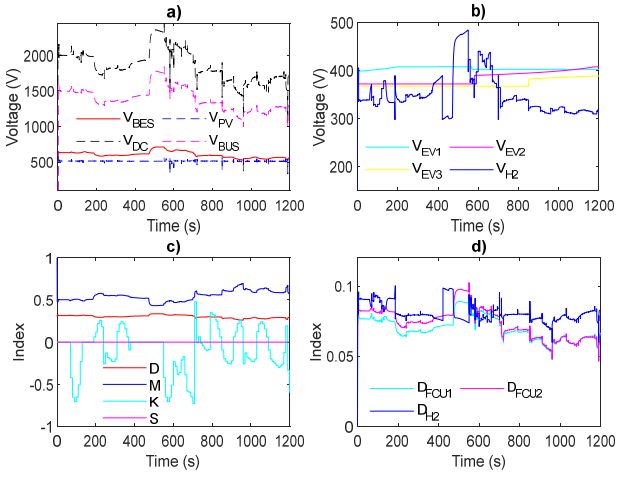

Fig. 7. a) BAT voltage, PV system voltage, DC voltage and MVDC bus voltage, b) hydrogen system voltage, and EV BAT voltages, c) *D* and *M* of the qZSI, *K* and *S* (outputs of the fuzzy logic block) and d) duty cycles of the DC/DC ZSC.

grid is to maintain the power balance in the system and obtain an economic benefit by selling energy to the grid. For example, at approximately 580 and 850 s, there is an excess of energy (P_{net}<0), and it can be observed that the fuzzy-logic-based system modifies the power used by the energy dispatch system ($P_{net,f}$ is closer to zero and there is less excess of energy) with the purpose of charging with lower power the BAT and hydrogen system and injecting power into the grid, taking advantage of the energy cost. Similarly, if there is a lack of energy (P_{net}>0), the fuzzy-logic-based system defines $P_{net,f}$ to absorb (or inject) energy from (into) the grid, and takes advantage of the energy cost again. In any case, the grid must compensate power peaks that neither the hydrogen system nor the BAT can generate (absorb). Fig. 6 is equivalent to Fig. 5, where the results obtained from the SCS proposed in [37] are illustrated. As demonstrated in that study, this SCS is also perfectly valid for this configuration of the MVDC microgrid for the charging of EVs.

The main voltages of the system are presented in Figs. 7a and 7b. In the case of V_{H2}, this voltage is a combination of LZ and FC voltages. For positive values of the net power, V_{H2} corresponds to the FC voltage (the LZ is disconnected), and for negative values, V_{H2} is the LZ voltage (the FC is disconnected). The switching indexes of the qZSI, D_{st} and M (shoot-through

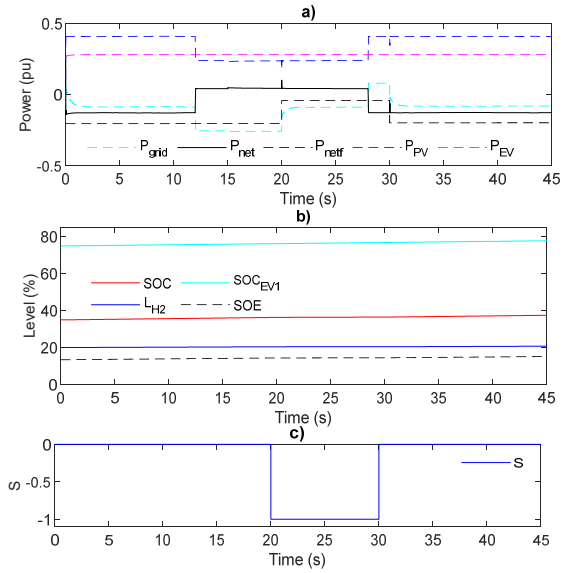

Fig. 8. Low *SOE* and P_{net}>0 a) grid power, PV system power, power demanded by the EV, P_{net} and $P_{net,f}$; b) BAT SOC, hydrogen tank level, *SOE*, and BAT SOC of the EV_1 ; and b) value of *S*.

duty cycle and index modulation, respectively) are shown in Fig. 7c. Moreover, Fig. 7d shows the duty cycle of the DC/DC ZSC. Note that, although there are two fast-charging units (two converters), three EVs are connected during the simulation. In these cases, a value of zero implies that there are not any EV connected to the converter. Similarly, if the duty cycle of the converter of the hydrogen system is zero, neither the LZ nor the FC is connected. The outputs of the fuzzy logic block (*K* and *S*) are shown in Fig. 7c. *K* modifies its value, and therefore, P_{net} changes depending on the value of C_{grid} (Fig. 4c), and the use of the grid improves. In contrast, because the SOE does not reach the extreme case in which S can be activated, its value remains constant throughout the simulation.

B. *Low SOE with Power Demand (P_{net}>0)*

This section shows how the SCS solves the situation of the MVDC microgrid when the *SOE* is low and there is a small power demand (P_{net}>0) simultaneously. Fig. 8 shows a 40 s-long simulation specifically designed for this purpose. In general, other SCS in the literature would avoid a further decrease in the *SOE*. Nevertheless, the SCS proposed herein, since the value of P_{net} can only be relatively small in this situation (see Table I), not only avoids a further reduction of the *SOE*, but also charges (if possible) both ESS and, therefore, increases the *SOE*. In Fig. 8a, between 12 s and 28 s, P_{net} is positive, corresponding to a power demand of 0.08 p.u, approximately. Until 12 s, P_{net} is negative and the SCS works as mentioned before. At 12 s, P_{net} becomes positive, and from 20 s on, *S* is activated according to the fuzzy logic rules (Fig. 8c) and $P_{net,f}$ becomes negative instead of the positive values of P_{net}. Despite the value of P_{net},

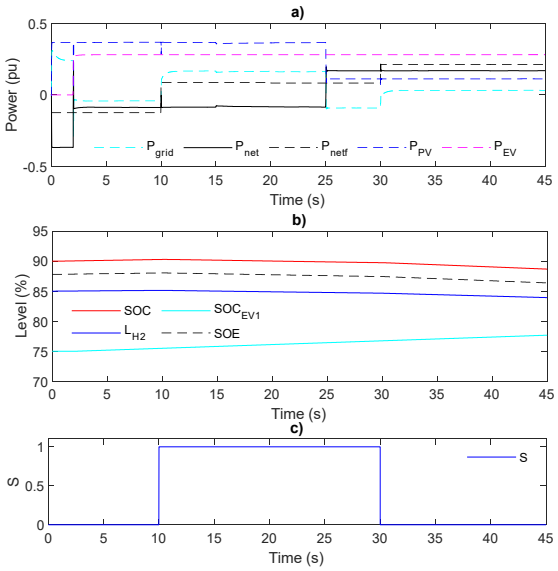

Fig. 9. High *SOE* and P_{net}<0: a) grid power, PV system power, power demanded by the EV, P_{net} and $P_{net,f}$; b) BAT SOC, hydrogen tank level, *SOE*, and c) value of *S*.

the *SOE* increases instead of decreasing (Fig. 8b). Note that the SCS updates $P_{net,f}$ every 10 s, and therefore, at 30 s, *S* is deactivated.

C. High SOE with Power Surplus (P_{net}<0)

This section corresponds to the opposite case studied in section IV.B. With a high *SOE* and P_{net}<0 the aim is to avoid an increase in *SOE*, despite the fact that there is an excess of power (again, relatively small as in Section IV.B.) *S* is activated between 10 s and 30 s (see Fig 9.) Therefore, the *SOE* decreases owing to the SCS and the fuzzy logic rules. During the first ten seconds there is an excess of power (P_{net}<0). At 10 s, the SCS detects it, and because the *SOE* is high, *S* is activated and P_{net} changes to a positive $P_{net,f}$. Because of this value of $P_{net,f}$, the *SOE* decreases and the *SOC* of the EV increases as usual despite the excess of power,. Finally, at 30 s, the SCS detects that P_{net} is positive, *S* is deactivated, and the SCS works as explained in Figs. 5-7.

D. Comparative Analysis

Table II illustrates the comparison between the SCS presented in this paper and the SCS developed in [37]. This table compares the economic benefit of both SCSs and the minimum and maximum values of *SOE*, *SOC* and L_{H2}. The economic benefit is calculated by considering the energy injected into the grid as revenue, and the energy consumed from it as expenditure. The results show that a total economic benefit of 166.1 € is obtained with the SCS presented in this paper (F-SCS), while this value is practically zero with the other SCS (Ref-SCS). In the F-SCS, the BAT and hydrogen system try to inject power into the grid to generate more revenue, and in the Ref-SCS, the grid only has to generate or absorb the peaks of power that neither the hydrogen system nor the BAT are able to balance. The use of the grid by the F-SCS makes the *SOE*, and therefore, the *SOC* and L_{H2} have, in general, lower levels than those of the Ref-SCS.

TABLE II. COMPARISON BETWEEN BOTH SCS

Term	F-SCS	REF-SCS
Economic benefit (€)	166,10 €	-6,65 €
SOC_{min} (%)	34,4	37,1
SOC_{max} (%)	89,6	93,7
$L_{H2,min}$ (%)	23,1	29,7
$L_{H2,max}$ (%)	65,9	77,7
SOE_{min} (%)	15,4	21,6
SOE_{max} (%)	77,7	84,3

E. Experimental Validation

Hardware-in-the-loop (HIL) allows testing and verifying the SCS in electric power systems, smart grids, and microgrids, without the need for complete system hardware. In HIL testing, a real-time plant emulator acts as a digital twin of the power system, whereas the control system is integrated into a digital board with a similar architecture as the final board to be used in the real system.

This section presents the results obtained from the HIL experimental validation. Fig. 10 show the setup built for the HIL configuration. It can be observed in the configuration used that the plant (grid-connected MVDC microgrid) and control run in real time in an OP4510 simulator from OPAL-RT, which is also used for monitoring the most relevant parameters in real time. The SCS is implemented in a dSPACE MicroLabBox unit, and dSPACE ControlDesk is used to monitor the signals of interest. In addition, a Yokogawa DLM4038 oscilloscope is used to capture and depict the most representative parameters in real-time (Fig. 11.) Fig. 11a shows the main powers of the system (P_{PV}, P_{BAT}, P_{H2}, P_{grid} and P_{EV}). These signals have been reduced to obtain values between -10 V and +10 V with a scale of 1 V/div. The EV power and PV system power are represented with an offset of -5 V. On the other hand, Fig. 11b shows the main voltages of the qZSI (V_{bus}, V_{PV}, V_{dc}, and V_{BAT}), the *SOE* and the indexes of the ZSVM technique, *M* and D_{st}. In this figure, in order to show all parameters in a single plot, the following setting has been reproduced: The voltage signals have been scaled down to obtain values between -10 V and +10 V with a scale of 1.25 V/div (offset of -5 V). The *SOE* has been scaled down to obtain values between -10 V and +10 V with a scale of 1 V/div (offset of -4 V). *M* and D_{st} have been scaled down to obtain values between -1 V and +1 V with a scale of 625 mV/div (offset of -2.6 V). The time scale is set to 50 s/div for all the signals in both figures.

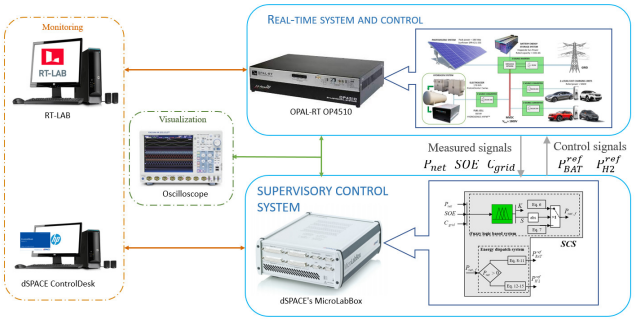

Fig. 10. Experimental setup implemented in this work

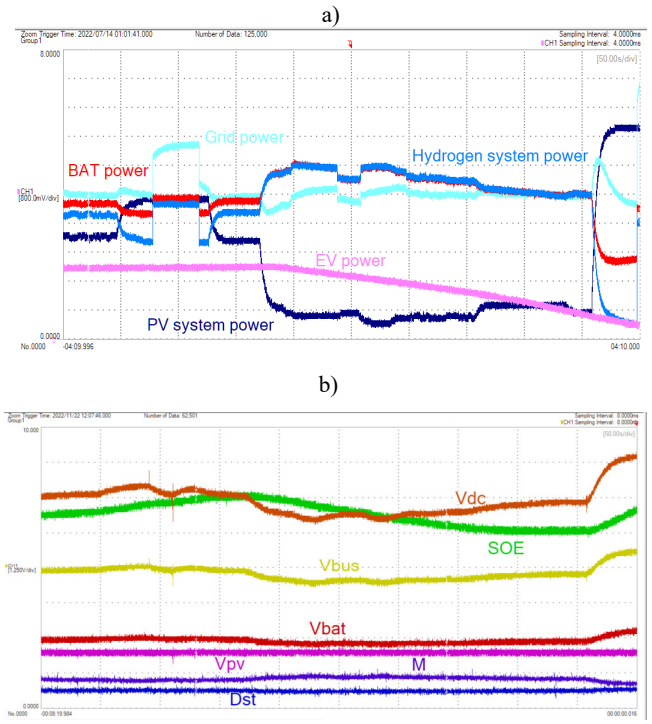

Fig. 11. Experimental results measured with the Yokogawa DLM4038 oscilloscope. a) main powers of the system, and b) main voltages in the qZSI, *SOE*, *M* and *Dst*

These captures show the first 500 s of the simulation with F-SCS. Thus, it can be verified that the PV system power and power demanded by the EV in Fig. 4a correspond to the shapes of the dark blue and pink signals of Fig. 11a. The same fact also occurs with the BAT, hydrogen system, and grid power in Fig. 5a and the red, blue, and light blue signals in Fig. 11a. Note that the difference between the PV system power and EV power is distributed among the BAT and the hydrogen system. In addition, between 75 s and 125 s, instead of using the ESSs to absorb the excess of the PV system power, the grid absorbs power to improve the economic benefit of the charging station. Regarding Fig. 11b, it can be observed that the main voltages in the system are properly regulated under variable sun irradiance; and the *SOE*, *M* and D_{st} are kept within adequate values, corresponding to the results registered in the simulation of the F-SCS. The results illustrate that the F-SCS works properly under the HIL experimental setup.

V. Conclusion

This paper described and evaluated a new SCS applied to a MVDC microgrid based on ZSC for an EV charging station. This work presented two main contributions: 1) the configuration of the MVDC microgrid by itself based on ZSC (composed of a PV system, BAT, hydrogen system, and grid), and 2) the design of the SCS based on a fuzzy-logic-based system to optimize the energy available in the hydrogen tank and the BAT, while maintaining the power balance and obtaining economic benefit from the use of the grid. Additionally, the SCS (F-SCS) was compared with a simpler SCS (Ref-SCS) previously presented in [37].

The results showed that the configuration proposed for the MVDC microgrid and the implemented SCS were perfectly valid for this application. In comparison, the economic benefit of the F-SCS was significant. Furthermore, the configuration allowed working with high levels of voltage (reducing currents) and reducing the number of converters used. Moreover, it was proved that the SCS maintained the power balance of the system, controlled the BAT SOC and the hydrogen tank level, and avoided the continued use of the local grid.

References

[1] European Commission, “CO2 emission performance standards for cars and vans (2020 onwards),” <https://ec.europa.eu/clima/policies/transport/vehicles/regulation_en > [accesed 01/11/2021].

[2] P. Vithayasrichareon, G. Mills, and I. F. MacGill, “Impact of electric vehicles and solar PV on future generation portfolio investment,” IEEE Trans. Sustain. energy, vol. 6, no. 3, pp. 899–908, April 2015.

[3] J. P. Torreglosa, P. García-Triviño, L. M. Fernández-Ramirez, and F. Jurado, “Decentralized energy management strategy based on predictive controllers for a medium voltage direct current photovoltaic electric vehicle charging station,” Energy Convers. Manag., vol. 108, pp. 1–13, Jan. 2016.

[4] P. García-Triviño, J. P. Torreglosa, L. M. Fernández-Ramírez, and F. Jurado, “Control and operation of power sources in a medium-voltage direct-current microgrid for an electric vehicle fast charging station with a photovoltaic and a battery energy storage system,” Energy, vol. 115, pp. 38–48, Nov. 2016,

[5] M. O. Badawy and Y. Sozer, “Power flow management of a grid tied PV-battery system for electric vehicles charging,” IEEE Trans. Ind. Appl., vol. 53, no. 2, pp. 1347–1357, Dec. 2016.

[6] P. García-Triviño, J. P. Torreglosa, F. Jurado, and L. M. F. Ramírez, “Optimised operation of power sources of a PV/battery/hydrogen-powered hybrid charging station for electric and fuel cell vehicles,” IET Renew. Power Gener., vol. 13, no. 16, pp. 3022–3032, Nov. 2019.

[7] S. Wang et al., "A Semi-Decentralized Control Strategy of a PV-based Microgrid with Battery Energy Storage Systems for Electric Vehicle Charging and Hydrogen Production," 2021 IEEE 4th International Electrical and Energy Conference (CIEEC), 2021, pp. 1-6.

[8] L. Wang, Z. Qin, T. Slangen, P. Bauer, and T. van Wijk, “Grid impact of electric vehicle fast charging stations: Trends, standards, issues and mitigation measures-an overview,” IEEE Open J. Power Electron., vol. 2, pp. 56–74, Jan. 2021.

[9] M. A. H. Rafi and J. Bauman, “A comprehensive review of DC fast-charging stations with energy storage: Architectures, power converters, and analysis,” IEEE Trans. Transp. Electrif., vol. 7, no. 2, pp. 345–368, August 2020.

[10] Afshari et al., “Control strategy for three-phase grid-connected PV inverters enabling current limitation under unbalanced faults,” IEEE Trans. Ind. Electron., vol. 64, no. 11, pp. 8908–8918, August 2017.

[11] Verma, B. Singh, A. Chandra, and K. Al-Haddad, “An Implementation of Solar PV Array Based Multifunctional EV Charger,” IEEE Trans. Ind. Appl., vol. 56, no. 4, pp. 4166–4178, August 2020.

[12] Hasabelrasul, Z. Cai, L. Sun, X. Suo, and I. Matraji, “Two-Stage Converter Standalone PV-Battery System Based on VSG Control,” IEEE Access, vol. 10, pp. 39825–39832, Jun. 2022.

[13] Y. Liu, H. Abu-Rub, B. Ge, F. Blaabjerg, O. Ellabban, and P. C. Loh, Impedance Source Power Electronic Converters. Hoboken, NJ, USA:Wiley, 2016.

[14] Chub, D. Vinnikov, R. Kosenko, E. Liivik, and I. Galkin, “Bidirectional DC–DC converter for modular residential battery energy storage systems,” IEEE Trans. Ind. Electron., vol. 67, no. 3, pp. 1944–1955, Mar. 2019.

[15] M. Ortega, M. V. Ortega, F. Jurado, J. Carpio, and D. Vera, “Bidirectional DC–DC converter with high gain based on impedance source,” IET Power Electron., vol. 12, no. 8, pp. 2069–2078, Mar. 2019.

[16] L. de Oliveira-Assis, E.P.P. Soares-Ramos, R. Sarrias-Mena, P. García-Triviño, E. González-Rivera, H. Sánchez-Sainz, F. Llorens-Iborra, L. M. Fernández-Ramírez, “Simplified model of battery energy-stored quasi-Z-

source inverter-based photovoltaic power plant with Twofold energy management system," Energy, vol. 244, Apr. 2022.
[17] Y. Zhang, P. You, and L. Cai, "Optimal Charging Scheduling by Pricing for EV Charging Station with Dual Charging Modes," IEEE Trans. Intell. Transp. Syst., vol. 20, no. 9, pp. 3386-3396, Sept. 2019.
[18] Y. Kim, J. Kwak, and S. Chong, "Dynamic Pricing, Scheduling, and Energy Management for Profit Maximization in PHEV Charging Stations," IEEE Trans. Veh. Technol., vol. 66, no. 2, pp. 1011-1026, Febr. 2017.
[19] C. Dou, D. Yue, X. Li and Y. Xue, "MAS-Based Management and Control Strategies for Integrated Hybrid Energy System," in IEEE Transactions on Industrial Informatics, vol. 12, no. 4, pp. 1332-1349, Aug. 2016.
[20] O. Elma, "A dynamic charging strategy with hybrid fast charging station for electric vehicles," Energy, vol. 202, p. 117680, Jul. 2020.
[21] D. A. Savio, V. A. Juliet, B. Chokkalingam, S. Padmanaban, J. B. Holm-Nielsen, and F. Blaabjerg, "Photovoltaic integrated hybrid microgrid structured electric vehicle charging station and its energy management approach," Energies, vol. 12, no. 1, Jan. 2019.
[22] L. Shen, Q. Cheng, Y. Cheng, L. Wei, and Y. Wang, "Hierarchical control of DC micro-grid for photovoltaic EV charging station based on flywheel and battery energy storage system," Electr. Power Syst. Res., vol. 179, p. 106079, Febr. 2020.
[23] T. Zhao, Y. Li, X. Pan, P. Wang, and J. Zhang, "Real-Time Optimal Energy and Reserve Management of Electric Vehicle Fast Charging Station: Hierarchical Game Approach," IEEE Trans. Smart Grid, vol. 9, no. 5, pp. 5357–5370, Mar. 2018.
[24] A. S. Mohamed et al., "Hierarchical Control of Megawatt-Scale Charging Stations for Electric Trucks with Distributed Energy Resources," IEEE Trans. Transp. Electrif., vol. 7782, no. c, pp. 1-13, Apr. 2022.
[25] Q. Chen, N. Liu, C. Hu, L. Wang, and J. Zhang, "Autonomous Energy Management Strategy for Solid-State Transformer to Integrate PV-Assisted EV Charging Station Participating in Ancillary Service," IEEE Trans. Ind. Informatics, vol. 13, no. 1, pp. 258-269, Nov. 2017.
[26] Zahedmanesh, K. M. Muttaqi, and D. Sutanto, "Active and Reactive Power Control of PEV Fast Charging Stations Using a Consecutive Horizon-Based Energy Management Process," IEEE Trans. Ind. Informatics, vol. 17, no. 10, pp. 6742–6753, Dec. 2021.
[27] Zahedmanesh, K. M. Muttaqi, and D. Sutanto, "A Cooperative Energy Management in a Virtual Energy Hub of an Electric Transportation System Powered by PV Generation and Energy Storage," IEEE Trans. Transp. Electrif., vol. 7, no. 3, pp. 1123-1133, Jan. 2021.
[28] Electric Vehicle Conductive Charging System_Part 1: General Requirements, document IEC 61851-1:2010, 2016.
[29] Suntech-Power. (2016). 265 Watt, STP265-20/WEM(265_260_255). [Online]. Available: http://www.suntechpower.com/menu/suntechproducts.html.
[30] HOPPECKE Batterien. (2017). Sun Power VR L Series OPzV. [Online]. Available: https://www.hoppecke.com/es/producto/grid-power-vr-l/.
[31] M. Kammerer (2014), "HyPMTM Fuel Cell Power Modules & Systems," in International Hydrail Conference, 2014, pp. 19–23, [Online]. Available: https://hydrail.appstate.edu/sites/hydrail.appstate.edu/files/9_Kammerer.pdf.
[32] ProtonOnsite. (2018). C Series. [Online]. Available: http://www.protononsite.com/sites/default/files/2017-07/PD-0600-0068-rev F.pdf
[33] L. de Oliveira-Assis, E. P. P. Soares-Ramos, R. Sarrias-Mena, P. García-Triviño and L. M. Fernández-Ramírez, "Large-Scale Grid Connected Quasi-Z-Source Inverter-Based PV Power Plant," 2020 IEEE International Conference on Environment and Electrical Engineering and 2020 IEEE Industrial and Commercial Power Systems Europe (EEEIC / I&CPS Europe), 2020, pp. 1-6.
[34] P. Garcia, L. M. Fernández, C. A. Garcia, and F. Jurado, "Comparative Study of PEM Fuel Cell Models for Integration in Propulsion Systems of Urban Public Transport," Fuel Cells, vol. 10, no. 6, pp. 1024-1039, Dec. 2010.
[35] R. Sarrias-Mena, L. M. Fernández-Ramírez, C. A. García-Vázquez and F. Jurado, "Electrolyzer models for hydrogen production from wind energy systems," Int. J. Hydrogen Energy, vol. 40, no. 7, pp. 2927–2938, Feb. 2015.
[36] M. Castañeda, A. Cano, F. Jurado, H. Sánchez, and L. M. Fernández, "Sizing optimization, dynamic modeling and energy management strategies of a stand-alone PV/hydrogen/battery-based hybrid system," Int. J. Hydrogen Energy, vol. 38, no. 10, pp. 3830–3845, Apr. 2013.
[37] P. García-Triviño, L. de Oliveira-Assis, E. P. P. Soares-Ramos, R. Sarrias-Mena, C. A. García-Vázquez, and L. M. Fernández-Ramírez, "Configuration and Control of a MVDC Hybrid Charging Station of Electric Vehicles with PV/Battery/Hydrogen System," in 2021 IEEE International Conference on Environment and Electrical Engineering and 2021 IEEE Industrial and Commercial Power Systems Europe (EEEIC/I&CPS Europe), 2021, pp. 1–5.
[38] Yazdani and R. Iravani, Voltage-sourced converters in power systems: modeling, control, and applications. Hoboken, New Jersey. John Wiley & Sons, 2010.

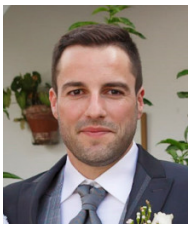

Pablo García-Triviño was born in La Línea de la Concepción, Cádiz, Spain, in 1984. He received the B.Sc. degree in Electrical Engineering, the M.Sc. degree in Industrial Engineering and the Ph.D. degree from the University of Cádiz, Cádiz, in 2005, 2007 and 2010, respectively.

Since 2008, he has been an Associate Professor with the Department of Electrical Engineering, University of Cádiz. His current research interests include power systems and power management in hybrid systems.

Laís de Oliveira-Assís was born in Belo Horizonte, Minas Gerais, Brazil in 1993. She received the B.Sc. degree in Energy Engineering from the Pontificia Universidade Catolica de Minas Gerais, Brazil, in 2017, with partial completion of an undergraduate program at Arizona State University, USA. She received the M.Sc. degree in Renewable Energy and Energy Efficiency in 2018, and the Ph.D. degree in Energy and Sustainable Engineering from the University of Cadiz, Spain, in 2022. Her research interests include renewable energy and energy storage systems.

Emanuel P. P. Soares-Ramos was born in Belo Horizonte, Minas Gerais, Brazil, in 1987. He graduated in Electrical Engineering, and he received M.Sc. degree in Electrical Power Systems from the Federal Center for Technological Education of Minas Gerais in 2012 and 2014, respectively. He received the Ph.D. degree in Energy and Sustainable Engineering from the University of Cadiz, Spain, in 2022.

He is a professor at the Engineering Department of Electro-electronics at the Federal Center for Technological Education, Minas Gerais. He is experienced in electrical engineering, working mainly on the following topics: renewable hybrid systems, protection of electrical systems, and electrical machines.

Raúl Sarrias-Mena was born in La Línea de la Concepción, Cádiz, Spain in 1985. He received the M.Sc. degree in Industrial Engineering and the Ph.D. degree from the University of Cádiz in 2010 and 2016, respectively.

He is currently an Assistant Professor at the Department of Engineering in Automation, Electronics, and Computer Architecture & Networks at the University of Cádiz, Spain. His research interests include regulation and control systems for hybrid renewable energy systems and energy storage systems.

Carlos Andrés García-Vázquez was born in La Línea de la Concepción, Cádiz, Spain. He received the M.Sc. degree in Engineering and the Ph.D. degree from the University of Cádiz, in 2004 and 2009, respectively.

Since 1988, he has been with the Department of Electrical Engineering at the University of Cadiz, Algeciras, Spain. He is currently an Associate Professor in the department. His research interests include electrical machines, renewable energy, and smart grids.

Luis M. Fernández-Ramírez (M'11–SM'15) was born in Los Barrios, Cádiz, Spain. He received the M.Sc. degree in Electrical Engineering from the University of Seville, Seville, Spain, in 1997, and a Ph.D. degree from the University of Cádiz, Cádiz, in 2004.

From 1997 to 2000, he was with the Department of Development and Research, Desarrollos Eólicos S.A. Seville. In 2000, he joined the University of Cádiz, where he is currently an Associate Professor with the Department of Electrical Engineering and Head of the Research Group in Sustainable and Renewable Electrical Technologies (PAIDI-TEP023). His research interests include smart grids, renewable energy, energy storage, hydrogen systems, electric vehicles, and power converters and control.